

Twisting a β -Carotene, an Adaptive Trick from Nature for Dissipating Energy during Photoprotection*

Received for publication, August 14, 2016, and in revised form, November 14, 2016. Published, JBC Papers in Press, December 19, 2016, DOI 10.1074/jbc.M116.753723

Manuel J. Llansola-Portoles^{‡1,2}, Roman Sobotka^{§1}, Elizabeth Kish^{‡1}, Mahendra Kumar Shukla[§], Andrew A. Pascal[‡], Tomáš Polívka[¶], and Bruno Robert[‡]

From the [‡]Institute for Integrative Biology of the Cell (I2BC), CEA, CNRS, Univ Paris-Sud, Université Paris-Saclay, F-91198, Gif-sur-Yvette cedex, France, the [§]Centre Algatech, Institute of Microbiology, Academy of Sciences of the Czech Republic, Třeboň, 379 81, Czech Republic, and the [¶]Institute of Physics and Biophysics, Faculty of Science, University of South Bohemia, České Budějovice 370 01, Czech Republic

Edited by James N. Siedow

Cyanobacteria possess a family of one-helix high light-inducible proteins (Hlips) that are homologous to light-harvesting antenna of plants and algae. An Hlip protein, high light-inducible protein D (HliD) purified as a small complex with the Ycf39 protein is evaluated using resonance Raman spectroscopy. We show that the HliD binds two different β -carotenes, each present in two non-equivalent binding pockets with different conformations, having their (0,0) absorption maxima at 489 and 522 nm, respectively. Both populations of β -carotene molecules were in all-trans configuration and the absorption position of the farthest blue-shifted β -carotene was attributed entirely to the polarizability of the environment in its binding pocket. In contrast, the absorption maximum of the red-shifted β -carotene was attributed to two different factors: the polarizability of the environment in its binding pocket and, more importantly, to the conformation of its β -rings. This second β -carotene has highly twisted β -rings adopting a flat conformation, which implies that the effective conjugation length N is extended up to 10.5 modifying the energetic levels. This increase in N will also result in a lower S_1 energy state, which may provide a permanent energy dissipation channel. Analysis of the carbonyl stretching region for chlorophyll α excitations indicates that the HliD binds six chlorophyll α molecules in five non-equivalent binding sites, with at least one chlorophyll α presenting a slight distortion to its macrocycle. The binding modes and conformations of HliD-bound pigments are discussed with respect to the known structures of LHCII and CP29.

In nature, photosynthetic organisms obtain their energy by collecting solar photons, using complex arrays of pigments known as antennas. Subsequently, the energy harvested by the antennas is transferred to reaction centers to be transduced into electrochemical potential. Finally after a cascade of molecular steps, this energy is stored as potential chemical energy that is easy to store and transport (1). To accomplish this pro-

cess, these organisms have developed a large number of different protein antenna assemblies, a notable subgroup of which are the light-harvesting complexes (LHCs)³ of green plants and algae. LHCs constitute a large family of proteins, which can exist as monomers, dimers, or trimers in the membrane, and have related amino acid sequences. It is hypothesized that in the evolution of photosynthesis there was, and continues to be, a selective advantage for the organism to make optimum use of low light conditions to drive the relatively slow downstream metabolic reactions of legacy biochemistry (2). Plants, algae, and cyanobacteria are oxygenic photosynthetic organisms that are exposed to random fluctuations in light intensity. In the case of low light requiring large antennas, during high light exposure, most of the energy absorbed is in excess of that required to drive downstream metabolism. If excess light energy is not dealt with properly, it may cause oxidative damage to the organism, mostly as the consequence of singlet oxygen generation. Hence it is vital for oxygenic photosynthetic organisms to develop mechanisms to deal with the abrupt overexposure to excess light and protect themselves from light-induced oxidative stress by dissipating excess absorbed energy as heat. Probably the most important of these mechanisms at a molecular level is the so-called nonphotochemical quenching. When photosynthetic activity is high, it induces a progressive acidification of the lumen because of the creation of the proton gradient, which in turn induces the presence of energy traps in the photosynthetic membrane (3, 4).

Nonphotochemical quenching is a complex regulatory mechanism, which is composed of diverse phases. The best-characterized phase is induced in seconds to minutes, and is called high-energy quenching (qE). During qE, energy traps may appear (or disappear) in seconds, thus originating from the re-organization of the photosynthetic membrane, and not from *de novo* synthesis of new proteins. The molecular mechanisms behind the qE process have been extensively discussed in the last decade, and although it is more and more generally admitted that the energy traps are localized in LHC proteins, several different hypotheses have been formulated about their chemical origin. Most of these hypotheses involve the LHC-bound

* This work was supported by the French National Infrastructure for Integrated Structural Biology (FRISBI) and Grants P501/12/G055 and 14-13967S from the Czech Science Foundation. The authors declare that they have no conflicts of interest with the contents of this article.

[†] These authors contributed equally to this work.

² To whom correspondence should be addressed. Tel.: 33-0-1-69-08-63-03; E-mail: manuel.llansola@cea.fr.

³ The abbreviations used are: LHC, light-harvesting complex; qE, high-energy quenching; Chl α , chlorophyll α ; Hlips, high light-inducible proteins; HliD, high light-inducible protein D.

carotenoid molecules, although it was also proposed that they arise from interacting chlorophyll molecules (5). Among the molecular mechanisms involving a carotenoid molecule, it was proposed that the quenching is induced by the reductive quenching of the chlorophyll α (Chl α) excited state via electron transfer to the carotenoid (6), by energy transfer quenching through singlet-singlet energy transfer from Chl α to the carotenoid (7), or by excitonic interaction between Chl α and the carotenoid (8).

Hlips are single-helix proteins (~ 7 kDa) ubiquitous in cyanobacteria that show significant sequence similarity to the first and third helices of eukaryotic LHCs. These small proteins possess a Chl α binding motif common to (and conserved among) all LHC proteins; and thus Hlips should be considered as members of the extended LHC superfamily (9–11). The genes that encode Hlips are strongly expressed under various stress conditions (12, 13), nevertheless, the exact role of Hlips in cells remains unclear. They are likely to play photoprotective and regulatory functions during synthesis and degradation of chlorophyll-binding proteins and during assembly and repair of Photosystem II (14). The cyanobacterium *Synechocystis* PCC 6083 contains four different Hlips (HliA–HliD) and all four of these small membrane proteins bind to early intermediates of the Photosystem II assembly (15, 16). Moreover, the HliD and HliC also form stable complexes with chlorophyll synthase, the terminal enzyme of Chl α biosynthesis (17, 18), and with the Ycf39 protein (15, 17). Ycf39 is a putative alcohol dehydrogenase with a conserved NADPH binding pocket but the exact role of this protein is not known yet. However, it has been already determined that the absence of this protein has a negative effect on the chlorophyll biosynthesis in *Synechocystis* (16).

The Ycf39-HliD complex was recently purified from *Synechocystis* and, because the Ycf39 itself does not bind pigments (15), the analysis of the Ycf39-HliD complex allowed for identification of certain spectroscopic properties of the HliD protein. The results revealed that HliD binds Chl α and β -carotene in a conformation that dissipates energy via singlet-singlet energy transfer from the Chl α Q_y state to the β -carotene S₁ state (19). Nevertheless, once the participation and the role of at least one of the two β -carotenes on the mechanism of energy dissipation were proven, the effect of the pigment configuration on the structure of the complex became crucial for the comprehension of the energy dissipation process. HliD binds Chl α and β -carotene with a stoichiometry of 3:1 (19). Fig. 1 proposes a model for HliD being a dimer binding six Chl α and two β -carotene molecules. In addition, it was shown in Staleva *et al.* (19) that at least one of the β -carotenes exhibits an extraordinary red-shifted absorption up to 550 nm, which may suggest that nature tailored a particular configuration and/or conformation of this β -carotene. Resonance Raman spectroscopy has been proven to be of great value to extract information on colored cofactors from biological materials as complex as the photosynthetic membrane, as it exhibits very high specificity through the resonance effect. Indeed, the Raman signal may be enhanced by up to 6 orders of magnitude when the frequency of the exciting light matches the energy of an electronic transition of the irradiated molecule. In a complex system containing many chromophores, the contribution of each chromophore to the

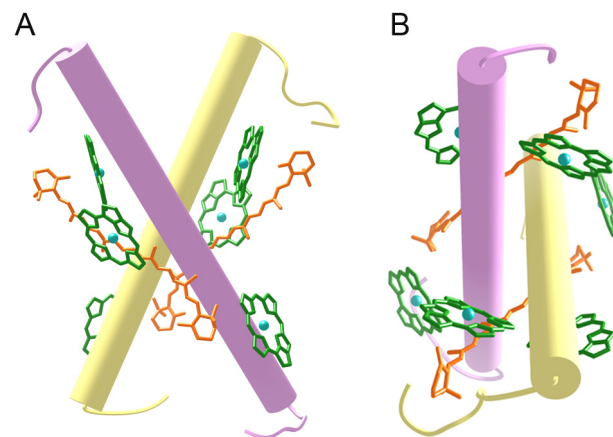


FIGURE 1. A model of the Chl α and β -carotene positions in the putative HliD dimer shown as a side view along the membrane plane (A) and a top view from the stromal side (B). The model was prepared using the crystal structure of pea LHCII (33). For clarity, only porphyrin rings of Chl molecules are shown.

Raman spectrum will depend on the excitation light. In systems containing more than one carotenoid the individual contribution of each molecule may be probed by controlling the precise frequency of the exciting beam. For example, this technique has been utilized for studies of the major LHC protein from higher plants, LHCII, which contains two luteins, one neoxanthin and up to one xanthophyll cycle carotenoid per monomer (20–22). Resonance Raman spectroscopy is also useful for analysis of the conformation, chemical, and intermolecular interactions of chlorophyll (23, 24).

In this work, we performed resonance Raman spectroscopy of the purified Ycf39-HliD complex at 77 K and room temperature with the aim of better understanding the role of pigment conformation in the molecular mechanisms that govern the fast fluorescence quenching. We identify and characterize the approximate number of Chl α and β -carotenes, and then analyze their configuration, conformation, and local environment in the HliD protein. The results are discussed with respect to the proposed structural model for this protein (19), and to the potential mechanisms underlying the dissipation process.

Results

Absorption Spectra of the Ycf39-HliD Complex—As there is no protocol yet how to isolate “pure” Hlips in quantities required for Raman spectroscopy we isolated the Ycf39-HliD complex via FLAG-tagged Ycf39 as described before (19). The absorption spectrum of the purified Ycf39-HliD complex measured at room temperature is shown in Fig. 2. It has a shape characteristic of an LHC absorption spectrum, consisting of Chl α Soret transitions with maxima at 436 and 420 nm and a Q_y band peaking at 675 nm. Absorbance shows two different peaks that can only arise from the bound β -carotene molecules. To minimize the error, we used second derivative analysis to determine the peak positions (Fig. 2, *inset*). One peak is observed at 492 nm, slightly red-shifted from β -carotene in *n*-hexane (478.2 nm), whereas the second peak is observed at 522 nm, with absorption extending up to 550 nm. These two absorption maxima have previously been attributed to two populations of

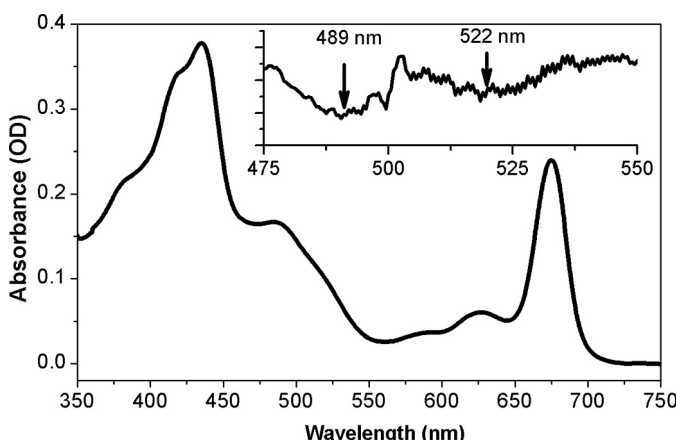


FIGURE 2. Absorption spectra of the Ycf39-HliD complex at room temperature. Inset, second derivative of absorption spectra at room temperature to identify the peak positions of the two β -carotenes.

β -carotene, called $\beta\text{-car}_1$ and $\beta\text{-car}_2$, respectively (19). We therefore attempted to determine whether these two β -carotene populations have different conformation and/or configuration in the protein, which may be responsible for these differences in absorption properties.

Resonance Raman of Chl α Molecules Bound to HliD—Resonance Raman spectra of Chl α molecules contain bands that arise from the vibrational modes coupled with the electronic transition used to produce the resonance effect, usually with the highest energy Soret band to avoid interference with the Chl α fluorescence (25). These modes often arise from vibrations delocalized on the Chl α macrocycle, some in the low frequency range (around 300 cm^{-1}), which involve the central magnesium atom, and others in the mid-frequency range ($800\text{--}1500\text{ cm}^{-1}$) sensitive to the Chl α macrocycle conformation (26). However, none of these modes in the low to mid frequencies undergo shifts large enough so that they can be used for conclusive analysis of pigment protein complexes containing as many chlorophylls as LHCs. The position of bands in the high-frequency region ($1500\text{--}1615\text{ cm}^{-1}$) is sensitive to the conformation of (bacterio)chlorophyll. The band around 1550 cm^{-1} , attributed to complex vibrational modes of the chlorin ring (27), along with the methine bridge stretching mode around 1600 cm^{-1} , are sensitive to the macrocycle core size and have been widely used to assess the number of axial ligands bound to the central magnesium of these molecules (26, 28). This methine bridge mode is observed at about 1600 cm^{-1} when the central magnesium is six-coordinated, and is up-shifted to $1610\text{--}1615\text{ cm}^{-1}$ for five-coordinated magnesium. Additionally, stretching modes of conjugated C = O groups (keto-carbonyl for Chl α) are observed above 1630 cm^{-1} (29). The keto stretching modes of Chl α contribute at about 1700 cm^{-1} when free from interaction in non-polar environments (30). This frequency downshifts up to 40 cm^{-1} when this group is involved in intermolecular interactions (H-bonds), the extent of the downshift being proportional to the strength of the interaction. Smaller downshifts occur ($5\text{--}10\text{ cm}^{-1}$) when the C = O is present in a polar environment.

Fig. 3 shows the resonance Raman spectra at 77 K of Ycf39-HliD, LHCII (31), and CP29 (31) excited at 413.1 nm (Table 1

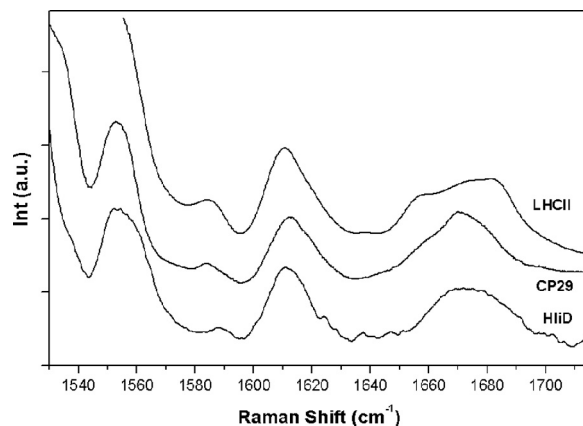


FIGURE 3. Resonance Raman spectra at 77 K excited at 413.1 nm for Ycf39-HliD, LHCII, and CP29.

TABLE 1

Frequencies of Chl α keto carbonyl stretching modes in CP29, LHCII, and HliD (in cm^{-1}), measured by resonance Raman spectroscopy

| CP29 | LHCII | HliD |
|-----------|-----------|-----------|
| | 1655 | |
| 1659 | 1659 | |
| 1665–1675 | 1670–1675 | 1666–1675 |
| 1685 | 1685 | 1682 |
| | 1700 | 1700 |

shows the frequencies of Chl α keto carbonyl stretching modes). In LHCII and CP29, modes sensitive to Chl conformation are localized around 1612 and 1550 cm^{-1} , indicating that the central magnesium atoms of most if not all Chl α molecules are five-coordinated in each case. These results were confirmed after comparing with the already resolved structure of LHCII (32, 33). In Ycf39-HliD, this shows a main component peaking at 1552 cm^{-1} and a clear additional component at 1558 cm^{-1} . This suggests that there is at least one Chl α with a distorted macrocycle attached to HliD. General distortions of the macrocycle, such as reduction of its core size generally affect the whole set of distortion-sensitive bands. In this case, we observed an additional component at 1558 cm^{-1} without any significant change in the band at 1612 cm^{-1} . It is thus likely that the distortion experienced by this Chl α concerns only a partial subset of the macrocycle angles between the pyrrole rings. In the keto carbonyl stretching mode region, the Ycf39-HliD complex presented a wide congested cluster of peaks at $1666\text{--}1675$, 1682.0 , and possibly one at 1695 cm^{-1} . Considering the intensity of the two latter bands, it is likely that at least four carbonyl modes contribute to the $1666\text{--}1675\text{ cm}^{-1}$ region, leading to a stoichiometry of at least six Chl α molecules, in fair agreement with the results of pigment analysis. For comparison, the spectra of CP29 and LHCII containing eight Chl α each are displayed in Fig. 3. It is of note that the population at 1659 cm^{-1} in LHCII and CP29, likely corresponding to two Chls α in each case and hypothesized to constitute a common structural motif for these proteins (31), is not present in the Ycf39-HliD spectrum.

Resonance Raman of β -Carotene Bound to HliD—Resonance Raman spectra of carotenoid molecules display four main groups of intense bands, which provide information on conformation and configuration for these molecules. One of the

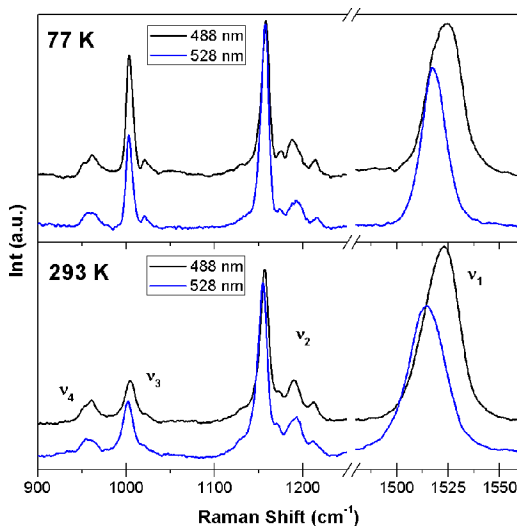


FIGURE 4. Resonance Raman spectra at 77 K (upper panel) and 293 K (lower panel) of the Ycf39-HliD complex (excited at 488.0 and 528.7 nm).

strongest bands in these spectra, contributing around 1530 cm^{-1} (referred to as ν_1), arises from stretching vibrations of the C = C bonds of the carotenoid. The frequency of this band is sensitive to the extent of the conjugated system of the scattering carotenoid and to its molecular configuration (34, 35); it also exhibits intrinsic temperature dependence (36). Fig. 4 shows the resonance Raman spectra at 77 and 293 K of Ycf39-HliD excited at 488.0 and 528.7 nm, corresponding to the maximum absorption for each of the β -carotenes determined in Fig. 2. At 528.7-nm excitation, which should favor the contribution of the red-most absorbing β -carotene ($\beta\text{-car}_2$), this band is observed at about 1516.9 cm^{-1} at 77 K and about 1514.3 cm^{-1} at room temperature. The bandwidth at 77 K is 12 cm^{-1} (FWHM), as it is expected for single carotenoid molecules. When moving the excitation to 488.0 nm, where resonance is expected with the blue-absorbing β -carotene ($\beta\text{-car}_1$), the frequency of this band shifts to 1523.8 and 1522.4 cm^{-1} at 77 K and room temperature, respectively. However, it is also clear that the band becomes much broader in these conditions of excitation (nearly 20 cm^{-1} , FWHM), revealing the presence of more than one carotenoid species contributing at this wavelength. Fig. 5a focuses on the 1500–1545 cm^{-1} region at 77 K for excitations at 488.0, 496.5, 501.7, 514.5, and 528.7 nm. These spectra can all be fitted with a linear combination of only two peaks, with maxima represented by dashed red lines at 1516.9 and 1526.9 cm^{-1} (data not shown). Hence, it can be concluded that there are only two β -carotene populations associated with the putative HliD dimer as suggested in Ref. 19 and that one of them displays an exceptionally red-shifted absorption. The 528.7 nm excitation fits with the 0–0 transition of $\beta\text{-car}_2$, and is lying far from the $\beta\text{-car}_1$. Shifting the excitation to the blue will result in a decrease of $\beta\text{-car}_2$ contributions, and an increase of those from $\beta\text{-car}_1$. However, the maximum 0–0 transition of the $\beta\text{-car}_1$ (~489 nm; Fig. 2) lies close to the expected position for the 0–1 transition of $\beta\text{-car}_2$ (33 nm from 522 nm). This will result in significant contributions of $\beta\text{-car}_2$ at 488.0 nm, as observed in Figs. 4 and 5.

The intense contributions around 1160 cm^{-1} , termed ν_2 , arise from stretching vibrations of C-C single bonds coupled

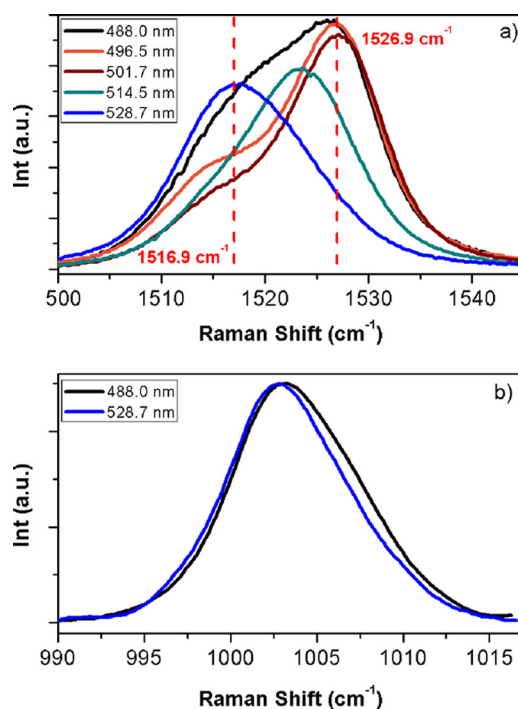


FIGURE 5. Resonance Raman spectra at 77 K of Ycf39-HliD. a, the 1500–1545 cm^{-1} region excited at 488.0, 514.5, and 528.7 nm. Vertical red dashed lines represent the center of the peaks corresponding to the two different β -carotenes. b, 990–10155 cm^{-1} region excited at 488.0 nm and 528.7 nm.

with C-H in-plane bending modes. This region is a fingerprint for the assignment of carotenoid configurations, *i.e.* isomerization states occurring in the conjugated C = C chain (34, 37). At room temperature, this region exhibits a main peak at 1155.2–1156.6 cm^{-1} with three satellite bands at 1171.6, 1190.2, and 1213.3 cm^{-1} , whereas at 77 K the main peak appears at 1157.9 cm^{-1} with the satellite bands at 1174.2, 1189.6, and 1214.8 cm^{-1} . These features do not present any difference from all-*trans* β -carotene in solution (34), and hence it may be safely concluded that the conjugated chain of both carotenoids present in HliD are in an all-*trans* configuration.

The next important set of bands appears around 1000 cm^{-1} (ν_3), arising from in-plane rocking vibrations of the methyl groups attached to the conjugated chain, coupled with the adjacent C-H in-plane bending modes (38, 39). It was proposed to be a fingerprint of the conjugated end cycle configuration (38), a hypothesis that was recently confirmed by theoretical modeling (39). For β -carotene in solvents, the band in ν_3 was shown as a doublet, and it was concluded that the presence of these two components revealed the out-of-plane configuration of the β -carotene end cycles (38). In Ycf39-HliD, this band (zoom-in Fig. 5b) displays mostly one component, located at 1003.2 cm^{-1} , when exciting at 528.7 nm, whereas two components are clearly observable upon 488.0 nm excitation, at 1002.7, and a shoulder at 1007.5 cm^{-1} , as observed for β -carotene free in solution (39, 40). Finally, around 960 cm^{-1} is found in the band termed ν_4 , which arises from C-H out-of-plane wagging motions coupled with C=C torsional modes (out-of-plane twists of the carbon backbone) (41). When the carotenoid-conjugated system is planar, these out-of-plane modes will not be coupled with the electronic transition, and these bands will not

Twisting a β -Carotene for Photoprotection

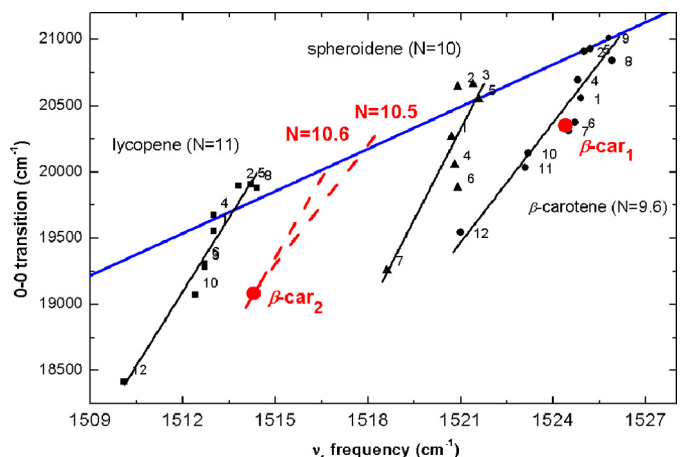


FIGURE 6. Correlation between the position of the $S_0 \rightarrow S_2$ electronic transition and the ν_1 band frequency, as a function of solvent polarizability, for β -carotene (black circles), spheroidene (black triangles), and lycopene (black squares). 1, tetrahydrofuran; 2, n-hexane; 3, dichloroethane; 4, cyclohexane; 5, diethyl ether; 6, toluene; 7, chloroform; 8, acetonitrile; 9, methanol; 10, pyridine; 11, nitrobenzene; 12, carbon disulfide. For comparison, the relationship between carotenoids of different conjugation lengths in the same solvent (n-hexane) is indicated by the blue line. The values for $\beta\text{-Car}_1$ and $\beta\text{-Car}_2$ in HLIID are indicated by red dots. All values were measured at room temperature.

be resonance-enhanced. However, distortions around C-C single bonds will increase the coupling of these modes with the electronic transition, resulting in an increase in their intensity, but also in their structure as these distortions will partially lift the degeneracy between the many ν_4 modes. In Fig. 4, it clearly appears that the ν_4 band displays a structure when exciting at both wavelengths: 488.0 nm ($\beta\text{-car}_1$) and 528.7 nm ($\beta\text{-car}_2$), indicating that both carotenoids are twisted. It is noteworthy that the structure observed for these bands is different. $\beta\text{-Car}_1$ presents an intense peak at 961 cm⁻¹ slightly more enhanced than the peak at this position for $\beta\text{-car}_2$.

To obtain further insight in the two β -carotenes attached to HLIID, we plotted the energy of the electronic transitions of the two bound carotenoids against the frequency of their ν_1 Raman band. Comparing simple, unsubstituted carotenoids on such a plot gives a linear relationship, where the position on the line depends on the effective conjugation length (42). Cyclic carotenoids such as β -carotene generally exhibit a shorter effective conjugation length than expected from their chemical structure, with the C-5,6 (and C-5',6') double bond(s) in the β -ring(s) adding only 0.3 to the effective conjugation length, N_{eff} , in each case, so that $N_{\text{eff}} = 9.6$ for β -carotene (42). On the other hand, for each carotenoid, the results obtained in different solvents fit with a different linear relationship, with the position on the line depending on the polarizability of their environment (42). This plot may thus give direct access to the effective conjugation length of a given carotenoid and the polarizability of its environment (42). In Fig. 6, the correlation between the position of the $S_0 \rightarrow S_2$ transition and the ν_1 band frequency, as a function of solvent polarizability was plotted for β -carotene (black circles, $N_{\text{eff}} = 9.6$), spheroidene (black triangles, $N_{\text{eff}} = 10$), and lycopene (black squares, $N_{\text{eff}} = 11$) in solution. The blue line represents the relationship between carotenoids of different conjugation length in the same solvent (n-hexane) (42). For each of these carotenoids, the correlation

between $S_0 \rightarrow S_2$ electronic transition and the ν_1 band frequency according to solvent polarizability was also plotted, represented as solid black lines. This correlation is similar for all carotenoid molecules, although it could be slightly less steep for β -carotene. When two β -carotenes present in Ycf39-HLIID are placed on the plot (red points), $\beta\text{-Car}_1$ fits on the line obtained for β -carotene according to solvent polarizability. This indicates that this molecule adopts the same configuration as in solvent, in an environment with moderate polarizability (similar to toluene). This conclusion is consistent with the analysis of the ν_3 components, where two components are observed at 488.0 nm, as for β -carotene in solution. Conversely, $\beta\text{-Car}_2$ clearly deviates from this line, and the relationship obtained between its absorption position and its ν_1 can only be interpreted by assuming that this molecule displays a longer effective conjugated length, and it is sitting in a relatively high polarizability environment. As the correlation according to solvent polarizability is not exactly the same for every carotenoid, taking into account the two extreme slopes (shown by the two red lines), we may propose that the effective length of $\beta\text{-Car}_2$ lies between 10.5 and 10.6 C=C, and the polarizability of its binding site is either (in the first case) very high, similar to carbon disulfide, or similar to toluene in the second case.

In solvent, β -carotene displays an effective conjugation length of 9.6, shorter than its 11 C=C-conjugated chain, and this was attributed to out-of-plane positions of its conjugated end-cycles due to torsional twisting of the terminal rings of carotenoids that contain conjugated C=C bonds (43, 44). We may thus further conclude that $\beta\text{-Car}_1$ in Ycf39-HLIID displays a configuration close to that observed in solvents, and is bound in a moderate polarizability binding site, whereas $\beta\text{-Car}_2$ have its C-5,6 (and C-5',6') double bonds in the β -rings clearly more conjugated to the π electronic system, and thus that its rings must be maintained close to the plane of the conjugated carbon chain. Its effective conjugation is close to that of its theoretically maximum ($n = 11$), and it is furthermore, bound to a binding site of high polarizability (comparable with carbon disulfide). It is well known that for terminal conjugated rings, the interaction of end groups with the polyene chain leads to steric deformations of around 45° for β -carotene (44). This deformation at the ends of the polyene chains together with the influence of end CH₃ groups or β -rings in carotenoids causes smaller participation of π orbitals from C₅ and C₆ atoms in HOMO and LUMO of the polyene chain, diminishing the effective conjugation length (44) as we observe for $\beta\text{-Car}_1$. On the other hand, the effective conjugation length of $\beta\text{-Car}_2$ (which is still lower than its theoretical conjugation length of 11) is determined in Fig. 6 by the ν_1 band position, which is 8 cm⁻¹ shifted from ν_1 band of $\beta\text{-Car}_1$. Bringing the aryl rings back into the plane of the β -carotene molecule would result in an increase of the effective conjugation length of up to 1.4. This effect has been observed for theoretical studies that prove that the change in dihedral angle of the terminal aryl ring in the ground state have an important effect in the effective conjugation length (43) and at the same time it has been observed for protein-bound carotenoids, where larger twists can be achieved depending on the design of the carotenoid binding pocket (45, 46). We thus propose that HLIID is able to tune the absorption of the red-absorbing β -carotene

via the rotation of its conjugated end-cycles toward the conjugated plane of the molecule, this rotation being imposed by its binding pocket through steric hindrance.

Discussion

The approach we use in this paper to address the structure and properties of the binding site of carotenoids, using a plot relating to energy of the electronic transition to the frequency of the C=C stretching mode, has already been widely applied to carotenoids bound to proteins (38, 42). It was shown, using this plot, that the absorption of carotenoid molecules in light-harvesting proteins from purple bacteria can be explained by the polarizability of their binding site alone. In that case, points corresponding to the LH-bound carotenoid in the plot obey the linear relationship due to solvent polarizability (38). In the case of the two luteins bound to LHCII and the two β -carotenes in Photosystem II reaction centers, polarizability alone can also explain the properties of the carotenoid molecule with absorption transitions to the blue. On the other hand, polarizability cannot explain the properties of the red-shifted carotenoid in either case, and an effect of the protein on their effective conjugation length had to be considered to account for the experimental results. Specific alterations of their equilibrium end-cycle conformations were concluded for the two red-absorbing carotenoids, in line with their ν_3 structure. It is important to emphasize that these conclusions were fully confirmed by analysis of the crystal structures of both proteins. However, for Photosystem II reaction centers, this effect is rather limited as the effective conjugation length reached by β -carotene is only 10 (38). It seems that the same phenomenon occurs for the HliD-bound β -Car₂, where the conjugation length increase up to about 10.5; the ν_3 band shows a clear shoulder indicating the twisting of both end rings and the shape of the ν_4 band when compared both carotenoids resembles that observed for the red-shifted β -carotene in Photosystem II reaction centers (38). Based on these similarities, it is possible to propose a model when the end rings of β -Car₂ are in a flat conjugated conformation, which has as a consequence the extension of the effective conjugation length.

HliD is a permanently quenched protein, and it has been clearly demonstrated that energy dissipation occurs via energy transfer from the Chl α Q_y state to β -carotene S₁ (19). Hence, these results suggest that this particularly extended conformation of the β -carotene molecule plays a role in the high efficiency of this singlet-singlet energy transfer.

The overall picture that emerges from this study is that the HliD binds two β -carotene molecules, both in S-cis configuration. The first one (β -Car₁) exhibits the same effective conjugation length as β -carotene in solution having moderate polarizability, whereas the second (β -Car₂) adopts an extended conformation that in turn confers to a molecule having lower energy of the S₀-S₂ transition. It is known that increase of the conjugation length leads to a decrease of energy of both the S₂ and S₁ states (47). Hence, it is proposed that this torsional conformation, which leads to an extension of effective conjugation, pushes the S₁ energy low enough to open a permanent dissipation channel for the excitation energy in this protein.

As shown previously the conformation of red-shifted β -carotene appears sensitive to the surrounding environment; the dissociation of Ycf39 from HliD changes the β -carotene absorption to be slightly less red-shifted (19). We, however, do not expect that the role Ycf39 is to modulate the HliD quenching mechanism. The firm binding of Ycf39 to HliD might rather localize this putative enzyme to a membrane compartment where it can regulate chlorophyll biosynthesis (17) and/or Photosystem II assembly (16). Structural details of the Ycf39 and HliD interaction are not known but the only feasible model is the Ycf39 binds to the N-terminal segment of HliD at the stromal side of the membrane (16). Indeed, the interaction with relatively large Ycf39 protein (40 kDa) will shape the HliD structure and probably also the β -carotene binding pocket.

We do not yet know whether there is an effect of Ycf39 on the efficiency of HliD quenching. However, the pure HliD clearly exhibits a quenching of chlorophyll fluorescence (19). Thus this quenching mechanism seems to be robust and not affected by small changes of carotenoid configuration. Nonetheless, the fact that the configuration of the quenching carotenoid in HliD can be affected by interactions with other proteins, or perhaps lipids, might play an important role during the evolution of eukaryotic antenna. A simple quenching mechanism in HliD seems adapted to a protein acting only for photoprotection. In LHCII from higher plants, which can oscillate from a light-harvesting mode to a quenching photoprotective mode, the dissipation mechanism is more complex, as it has to be tuned according to photosynthetic activity.

Experimental Procedures

Sample Preparation—Construction of *Synechocystis* strains and purification of the Ycf39-HliD complex were completed as described in Ref. 19.

Absorption Spectroscopy—Absorption spectra were collected using a Varian Cary E5 Double-beam scanning spectrophotometer.

Raman Spectroscopy—Resonance Raman spectra were recorded with a 90° signal collection using a two-stage monochromator (U1000, Jobin Yvon, Longjumeau, France) equipped with a front-illuminated, deep-depleted CCD detector (Jobin Yvon, Longjumeau, France). Excitation wavelengths were provided by a 24-watt Sabre Argon laser (Coherent, Palo Alto, CA), except for 413.1 and 406.7 nm, which were provided by an Innova 90 Krypton laser (Coherent). Unless otherwise indicated, less than 2 milliwatts reached the sample, and the sample integrity was verified by following resonance Raman spectral evolution during the experiment. These experiments were done at 77 K in an LN₂ flow cryostat (Air Liquide), and room temperature and the spectral resolution of the Raman spectrometer was 0.5 cm⁻¹.

Author Contributions—M. K. S purified the Ycf39-HliD complex. M. J. L. P., R. S., and E. K. contributed in the acquisition, analysis, preparation of the manuscript, and interpretation of data; A. P., T. P., and B. R. contributed to the preparation of the manuscript.

References

- Blankenship, R. E. (2014) *Molecular Mechanisms of Photosynthesis*, Blackwell Science, Oxford, United Kingdom

Twisting a β -Carotene for Photoprotection

2. Gust, D., Kramer, D., Moore, A., Moore, T. A., and Vermaas, W. (2008) Engineered and artificial photosynthesis: human ingenuity enters the game. *MRS Bull.* **33**, 383–387
3. Demmig-Adams, B., Garab, G., Adams Iii, W., and Govindjee. (2014) *Non-Photochemical Quenching and Energy Dissipation in Plants, Algae and Cyanobacteria*, Springer, The Netherlands
4. Ruban, A. V. (2016) Nonphotochemical chlorophyll fluorescence quenching: mechanism and effectiveness in protecting plants from photodamage. *Plant Physiol.* **170**, 1903–1916
5. Müller, M. G., Lambrev, P., Reus, M., Wientjes, E., Croce, R., and Holzwarth, A. R. (2010) Singlet energy dissipation in the photosystem II light-harvesting complex does not involve energy transfer to carotenoids. *ChemPhysChem* **11**, 1289–1296
6. Holt, N. E., Zigmantas, D., Valkunas, L., Li, X.-P., Niyogi, K. K., and Fleming, G. R. (2005) Carotenoid cation formation and the regulation of photosynthetic light harvesting. *Science* **307**, 433–436
7. Ruban, A. V., Berera, R., Illoiaia, C., van Stokkum, I. H., Kennis, J. T., Pascal, A. A., van Amerongen, H., Robert, B., Horton, P., and van Grondelle, R. (2007) Identification of a mechanism of photoprotective energy dissipation in higher plants. *Nature* **450**, 575–578
8. Bode, S., Quentmeier, C. C., Liao, P.-N., Hafi, N., Barros, T., Wilk, L., Bittner, F., and Walla, P. J. (2009) On the regulation of photosynthesis by excitonic interactions between carotenoids and chlorophylls. *Proc. Natl. Acad. Sci. U.S.A.* **106**, 12311–12316
9. Dolganov, N. A., Bhaya, D., and Grossman, A. R. (1995) Cyanobacterial protein with similarity to the chlorophyll *a/b* binding proteins of higher plants: evolution and regulation. *Proc. Natl. Acad. Sci. U.S.A.* **92**, 636–640
10. Neilson, J. A., and Durnford, D. G. (2010) Structural and functional diversification of the light-harvesting complexes in photosynthetic eukaryotes. *Photosynth. Res.* **106**, 57–71
11. Engelken, J., Brinkmann, H., and Adamska, I. (2010) Taxonomic distribution and origins of the extended LHC (light-harvesting complex) antenna protein superfamily. *BMC Evol. Biol.* **10**, 233
12. Bhaya, D., Dufresne, A., Vaulot, D., and Grossman, A. (2002) Analysis of the *hli* gene family in marine and freshwater cyanobacteria. *FEMS Microbiol. Lett.* **215**, 209–219
13. He, Q., Dolganov, N., Bjorkman, O., and Grossman, A. R. (2001) The high light-inducible polypeptides in *Synechocystis* PCC6803: expression and function in high light. *J. Biol. Chem.* **276**, 306–314
14. Komenda, J., and Sobotka, R. (2016) Cyanobacterial high-light-inducible proteins: protectors of chlorophyll: protein synthesis and assembly. *Biochim. Biophys. Acta* **1857**, 288–295
15. Yao, D., Kieselbach, T., Komenda, J., Promnares, K., Prieto, M. A., Tichy, M., Vermaas, W., and Funk, C. (2007) Localization of the small CAB-like proteins in photosystem II. *J. Biol. Chem.* **282**, 267–276
16. Knoppová, J., Sobotka, R., Tichy, M., Yu, J., Koník, P., Halada, P., Nixon, P. J., and Komenda, J. (2014) Discovery of a chlorophyll binding protein complex involved in the early steps of photosystem II assembly in *Synechocystis*. *Plant Cell* **26**, 1200–1212
17. Chidgey, J. W., Linhartová, M., Komenda, J., Jackson, P. J., Dickman, M. J., Canniffe, D. P., Koník, P., Pilný, J., Hunter, C. N., and Sobotka, R. (2014) A cyanobacterial chlorophyll synthase-HliD complex associates with the Ycf39 protein and the YidC/Alb3 insertase. *Plant Cell* **26**, 1267–1279
18. Niedzwiedzki, D. M., Tronina, T., Liu, H., Staleva, H., Komenda, J., Sobotka, R., Blankenship, R. E., and Polívka, T. (2016) Carotenoid-induced non-photochemical quenching in the cyanobacterial chlorophyll synthase-HliC/D complex. *Biochim. Biophys. Acta* **1857**, 1430–1439
19. Staleva, H., Komenda, J., Shukla, M. K., Šlouf, V., Kaňa, R., Polívka, T., and Sobotka, R. (2015) Mechanism of photoprotection in the cyanobacterial ancestor of plant antenna proteins. *Nat. Chem. Biol.* **11**, 287–291
20. Ruban, A. V., Lee, P. J., Wentworth, M., Young, A. J., and Horton, P. (1999) Determination of the stoichiometry and strength of binding of xanthophylls to the photosystem II light harvesting complexes. *J. Biol. Chem.* **274**, 10458–10465
21. Ruban, A. V., Pascal, A. A., Robert, B., and Horton, P. (2001) Configuration and dynamics of xanthophylls in light-harvesting antennae of higher plants: spectroscopic analysis of isolated light-harvesting complexes of photosystem II and thylakoid membranes. *J. Biol. Chem.* **276**, 24862–24870
22. Ruban, A. V., Pascal, A., Lee, P. J., Robert, B., and Horton, P. (2002) Molecular configuration of xanthophyll cycle carotenoids in photosystem II antenna complexes. *J. Biol. Chem.* **277**, 42937–42942
23. Robert, B. (1996) Resonance Raman studies in photosynthesis: chlorophyll and carotenoid molecules. in *Biophysical Techniques in Photosynthesis* (Amesz, J., and Hoff, A., eds) pp. 161–176, Springer, The Netherlands
24. Pascal, A. A., Ruban, A. V., and Robert, B. (2014) Antenna protein conformational changes revealed by resonance Raman spectroscopy. in *Non-Photochemical Quenching and Energy Dissipation in Plants, Algae and Cyanobacteria* (Demmig-Adams, B., Garab, G., Adams, Iii, W., and Govindjee, eds) pp. 245–257, Springer, The Netherlands
25. Lutz, M. (1977) Antenna chlorophyll in photosynthetic membranes: a study by resonance Raman spectroscopy. *Biochim. Biophys. Acta* **460**, 408–430
26. Fujiwara, M., and Tasumi, M. (1986) Metal-sensitive bands in the Raman and infrared spectra of intact and metal-substituted chlorophyll *a*. *J. Phys. Chem.* **90**, 5646–5650
27. Lutz, M., and Mäntele, W. (1991) in *The Chlorophylls* (Scheer, H., ed) pp. 855–902, CRC Press Inc., Boca Raton, FL
28. Näveke, A., Lapouge, K., Sturgis, J. N., Hartwich, G., Simonin, I., Scheer, H., and Robert, B. (1997) Resonance Raman spectroscopy of metal-substituted bacteriochlorophylls: characterization of Raman bands sensitive to bacteriochlorin conformation. *J. Raman Spectrosc.* **28**, 599–604
29. Feiler, U., Mattioli, T. A., Katheder, I., Scheer, H., Lutz, M., and Robert, B. (1994) Effects of vinyl substitutions on resonance Raman spectra of (bacterio)chlorophylls. *J. Raman Spectrosc.* **25**, 365–370
30. Lapouge, K., Näveke, A., Sturgis, J. N., Hartwich, G., Renaud, D., Simonin, I., Lutz, M., Scheer, H., and Robert, B. (1998) Non-bonding molecular factors influencing the stretching wavenumbers of the conjugated carbonyl groups of bacteriochlorophyll *a*. *J. Raman Spectrosc.* **29**, 977–981
31. Pascal, A., Wacker, U., Irrgang, K.-D., Horton, P., Renger, G., and Robert, B. (2000) Pigment binding site properties of two photosystem II antenna proteins: a resonance Raman investigation. *J. Biol. Chem.* **275**, 22031–22036
32. Liu, Z., Yan, H., Wang, K., Kuang, T., Zhang, J., Gui, L., An, X., and Chang, W. (2004) Crystal structure of spinach major light-harvesting complex at 2.72 Å resolution. *Nature* **428**, 287–292
33. Standfuss, J., Terwisscha van Scheltinga, A. C., Lamborghini, M., and Kühlbrandt, W. (2005) Mechanisms of photoprotection and nonphotochemical quenching in pea light-harvesting complex at 2.5-Å resolution. *The EMBO J.* **24**, 919–928
34. Robert, B. (1999) The electronic structure, stereochemistry and resonance Raman spectroscopy of carotenoids. in *The Photochemistry of Carotenoids* (Frank, H. A., Young, A. J., Britton, G., and Cogdell, R. J., eds) pp. 189–201, Springer, The Netherlands
35. Koyama, Y., and Fujii, R. (1999) Cis-trans carotenoids in photosynthesis: configurations, excited-state properties and physiological functions. in *The Photochemistry of Carotenoids* (Frank, H. A., Young, A. J., Britton, G., and Cogdell, R. J., eds) pp. 161–188, Springer, The Netherlands
36. Andreeva, A., Apostolova, I., and Velitchkova, M. (2011) Temperature dependence of resonance Raman spectra of carotenoids. *Spectrochim. Acta A Mol. Biomol. Spectrosc.* **78**, 1261–1265
37. Koyama, Y., Takii, T., Saiki, K., and Tsukida, K. (1983) Configuration of the carotenoid in the reaction centers of photosynthetic bacteria: 2. comparison of the resonance Raman lines of the reaction centers with those of the 14 different cis-trans isomers of β -carotene. *Photochem. Photobiol.* **5**, 139–150
38. Mendes-Pinto, M. M., Galzerano, D., Telfer, A., Pascal, A. A., Robert, B., and Illoiaia, C. (2013) Mechanisms underlying carotenoid absorption in oxygenic photosynthetic proteins. *J. Biol. Chem.* **288**, 18758–18765
39. Macernis, M., Galzerano, D., Sulskus, J., Kish, E., Kim, Y.-H., Koo, S., Valkunas, L., and Robert, B. (2015) Resonance Raman spectra of carotenoid molecules: influence of methyl substitutions. *J. Phys. Chem. A* **119**, 56–66

40. Telfer, A., Frolov, D., Barber, J., Robert, B., and Pascal, A. (2003) Oxidation of the two β -carotene molecules in the photosystem II reaction center. *Biochemistry* **42**, 1008–1015
41. Lutz, M., Szponarski, W., Berger, G., Robert, B., and Neumann, J.-M. (1987) The stereoisomerization of bacterial, reaction-center-bound carotenoids revisited: an electronic absorption, resonance Raman and NMR study. *Biochim. Biophys. Acta* **894**, 423–433
42. Mendes-Pinto, M. M., Sansiaume, E., Hashimoto, H., Pascal, A. A., Gall, A., and Robert, B. (2013) Electronic absorption and ground state structure of carotenoid molecules. *J. Phys. Chem. B* **117**, 11015–11021
43. Fuciman, M., Keşan, G., LaFountain, A. M., Frank, H. A., and Polívka, T. (2015) Tuning the spectroscopic properties of aryl carotenoids by slight changes in structure. *J. Phys. Chem. B* **119**, 1457–1467
44. Macernis, M., Sulskus, J., Malickaja, S., Robert, B., and Valkunas, L. (2014) Resonance Raman spectra and electronic transitions in carotenoids: a density functional theory study. *J. Phys. Chem. A* **118**, 1817–1825
45. Polívka, T., Kerfeld, C. A., Pascher, T., and Sundström, V. (2005) Spectroscopic properties of the carotenoid 3'-hydroxyechinenone in the orange carotenoid protein from the cyanobacterium *Arthrospira maxima*. *Biochemistry* **44**, 3994–4003
46. Polívka, T., Balashov, S. P., Chábera, P., Imasheva, E. S., Yartsev, A., Sundström, V., and Lanyi, J. K. (2009) Femtosecond carotenoid to retinal energy transfer in xanthorhodopsin. *Biophys. J.* **96**, 2268–2277
47. Polívka, T., and Sundström, V. (2004) Ultrafast dynamics of carotenoid excited states: from solution to natural and artificial systems. *Chem. Rev.* **104**, 2021–2071

Twisting a β -Carotene, an Adaptive Trick from Nature for Dissipating Energy during Photoprotection

Manuel J. Llansola-Portoles, Roman Sobotka, Elizabeth Kish, Mahendra Kumar Shukla,
Andrew A. Pascal, Tomás Polívka and Bruno Robert

J. Biol. Chem. 2017, 292:1396-1403.

doi: 10.1074/jbc.M116.753723 originally published online December 19, 2016

Access the most updated version of this article at doi: [10.1074/jbc.M116.753723](https://doi.org/10.1074/jbc.M116.753723)

Alerts:

- When this article is cited
- When a correction for this article is posted

[Click here](#) to choose from all of JBC's e-mail alerts

This article cites 40 references, 15 of which can be accessed free at
<http://www.jbc.org/content/292/4/1396.full.html#ref-list-1>